Journal of Engineering and Technological Sciences

Numerical Solution of nth Order DAEM for Kinetic Study of Lignocellulosic Biomass Pyrolysis

Jonas Kristanto¹, Muhammad Mufti Azis^{1,*} & Suryo Purwono^{1,2}

¹Department of Chemical Engineering, Faculty of Engineering, Universitas Gadjah Mada, Jalan Grafika 2, Yogyakarta, 55281, Indonesia

²Professional Engineering Program, Faculty of Engineering, Universitas Gadjah Mada, Jalan Grafika 2, Yogyakarta, 55281, Indonesia

Corresponding author: muhammad.azis@ugm.ac.id

Abstract

The aim of the present study was to explore the most optimal configuration to numerically solve Distributed Activation Energy Models (DAEMs). DAEMs are useful in obtaining the kinetic parameters in non-isothermal kinetic studies using a thermogravimetry analyzer (TGA). Compared to other kinetic models, DAEMs provide an additional kinetic parameter that quantifies the extent of the reaction (σ) for each reaction's mean activation energy (E'). Although DAEMs are efficacious in kinetic studies, solving DAEMs numerically is challenging. The DAEM equation includes double integration with respect to activation energy and temperature, which involves various numerical discretizations. Previously, many researchers utilized a DAEM to explicate complex reactions such as lignocellulosic biomass pyrolysis. However, most of them have yet to propose a numerical approach to solve DAEMs. Therefore, by exploring multiple numerical calculation configurations, here we present a general structure to numerically solve nth order and first-order DAEMs. The exploration includes determining the optimal integration limit of activation energy and the discretization of activation energy and temperature integration. From the investigation, we came up with a configuration that limits the integration of activation energy from E-3 σ to E+3 σ . Meanwhile, the number of integration points for temperature and activation energy must be 51 and 21, respectively. By using this configuration, DAEM can be utilized optimally in kinetic studies.

Keywords: DAEM; kinetics; lignocellulosic biomass pyrolysis; numerical calculation; TGA.

Introduction

Pyrolysis is a thermal processing reaction to convert feedstocks to gaseous, liquid, and solid products [1,2]. It is usually conducted in an oxygen-free vessel such as a fixed-bed reactor [3], fluidized-bed reactor [4], thermogravimetry analyzer (TGA) with continuous supply of inert gas [5], or custom-made pyrolizer [6]. Among these options, TGA is one of the most commonly used instruments to predict the kinetic parameters of pyrolysis [7]. TGA operates non-isothermally under a linearly changing temperature program. The linear increase of temperature combined with weight loss data aids researchers in developing a kinetic model of the pyrolysis reaction.

In general, kinetic studies of thermogravimetric reactions such as pyrolysis can be divided into two methods: model-free and model-fitting. Model-free, or iso-conversional, methods are typically implemented in the form of the Kissinger-Akahira-Sunose (KAS) [8], Ozawa-Flynn-Wall (OFW) [9], and Friedman [10] methodologies. These were developed around 1960 from the assumption that at a certain degree of conversion, a reaction has a certain value of activation energy. On using the model-free methodology, the researcher needs to provide data for multiple heating rates. Most commonly, researchers employ data from three to five different heating rates [11-14] to achieve reliable kinetic parameters [15]. By using these data, the activation energy trend can be obtained by regressing the temperature and the heating rate value at a certain degree of conversion [16] or at the maximum reaction rate, as in Coats-Redfern's methodology [17]. However, the model-free method also comes with limitations. To begin with, the methodology provides a trend of kinetic parameters that only give us an indication of the occurrence of a multi-stage reaction [15,18]. From this first limitation, it is impossible for researchers to deconvolute the multi-stage reaction. Secondly, the model-free methodology can only be

Copyright ©2023 Published by IRCS - ITB ISSN: 2337-5779

J. Eng. Technol. Sci. Vol. 55, No. 3, 2023, 261-274 DOI: 10.5614/j.eng.technol.sci.2023.55.3.4

implemented with a system that neglects heat transfer. In a system with rapid change in temperature or a sample with a large volume, heat transfer should be accounted for and cannot be neglected. A model-free kinetic analysis in this kind of system will produce an invalid result. This is because the heat transfer phenomenon will be compensated by the calculated kinetic parameters.

To properly model a complex multi-stage reaction such as pyrolysis, a model-fitting method provides more room for exploration, especially for complex reactions. The model-fitting method basically requires the user to propose an initial assumption in the form of a proposed model to be fitted to the experimental data. There are various types of models that can be fitted to the experimental data – from the classical power law model to DAEM. However, applying the conventional power law model to a complex reaction such as lignocellulosic biomass pyrolysis is insufficient. Since biomass has different kinds of atomic bonds in it, using the power law model to explicate the pyrolysis of biomass will eventually require multiple independent equations to represent each reaction sequence.

In most recent studies, the model-fitting kinetic study of biomass pyrolysis employed DAEM [19]. DAEM is commonly found in pyrolysis kinetic studies and has proven to be a powerful tool to simplify and deconvolute the complex multi-stage reaction of biomass [18,20-23] or coal [24]. In these studies, the kinetic analysis was performed by coupling non-linear regression to obtain the most suitable parameter values. In the analyses, it is common to use the sum squared of errors/residuals (SSE), the sum squared due to regression (SSR), or the coefficient of determination (R²) to evaluate the suitability of the result. However, there are no limits to how low or high the value to consider the validity of the analysis.

Although DAEM provides many possibilities to study the kinetics of a reaction, DAEM has an intricate mathematical form that makes it hard to solve analytically. In 2002, a numerical algorithm was developed to solve DAEM directly [24]. The algorithm provided a strategy to solve DAEM with direct numerical calculation. However, the methodology still lacks in detail, especially in the calculation configuration. In solving DAEM with numerical calculation, one needs to determine the number of numerical integration points and integration range of activation energy and temperature. In the previous algorithm, the upper limit of activation energy was set at 500 kJ mol⁻¹ with fifty integration interval steps [24]. However, this approach is not efficient since most activation energy of thermogravimetric pyrolysis lies between 100 to 270 kJ mol⁻¹ [18,20,25]. In more detail, a large interval will produce a skewed curve and an inaccurate result. Meanwhile, a large integration range will present an extraneous calculation that is far outside the common activation range of lignocellulosic biomass pyrolysis. In addition, the number of temperature integration points and the range have not been explained explicitly in the same publication [24].

Overall, the numerical solution of DAEM has been previously explored by other researchers. However, they did not provide a detailed strategy to solve it. Hence, to provide a better insight into directly solving DAEM with a numerical calculation, this work aimed to provide a more detailed strategy to solve DAEM by investigating many configurations. In this work, we investigated the influence of temperature data points, the number of numerical integration points for activation energy and temperature, as well as the influence of the integration range for the activation energy. A comparison between each calculation configuration is presented in the form of the statistical parameters and simulation time required to solve the calculation. Furthermore, we also explored the effect of various heating rates on the shape of the Derivative Thermogravimetric (DTG) curve that is produced from direct numerical solution of DAEM. From this exploration of the DAEM calculation configuration, we hope to provide a better understanding of the application of DAEM in future kinetic studies of thermogravimetric lignocellulosic biomass pyrolysis.

Materials and Methodology

Materials

In this work, the calculation was conducted on Spyder (Python 3.9) that was released under Anaconda Distribution. All simulations were conducted using an Apple MacBook Air (M1, 2020) MGN63ID/A with 8 GB of Unified Memory and a Solid-State Drive of 256 GB.

Equation of Distributed Activation Energy Model (DAEM)

DAEM has been widely used and there are multiple examples of its derivation and mathematical proof in the literature. Overall, there are two different forms of DAEM, as shown in Eqs. (1) and (2):

$$\frac{d\alpha}{dT} = \int_0^\infty \left\{ \frac{k_0}{\beta} \exp\left(-\frac{E}{RT}\right) \left[1 - (1 - n)\frac{k_0}{\beta} \int_{T_0}^T \exp\left(-\frac{E}{RT}\right) dT\right]^{\frac{n}{1 - n}} \right\} f(E) dE \tag{1}$$

$$\frac{d\alpha}{dT} = \int_0^\infty \left\{ \frac{k_0}{\beta} \exp\left[-\left(\frac{E}{RT} + \frac{k_0}{\beta} \int_{T_0}^T \exp\left(-\frac{E}{RT} \right) dT \right) \right] \right\} f(E) dE \tag{2}$$

$$f(E) = \frac{1}{\sigma\sqrt{2\pi}} \exp\left[-\frac{1}{2} \left(\frac{E - \bar{E}}{\sigma}\right)^2\right] \tag{3}$$

The first equation applies to reactions with order of reaction other than one, whereas the second is applicable to first-order reactions. In addition, to support both equations, it is pivotal to integrate a certain form of selected distribution function. Many publications on kinetic analysis with DAEM used a common Gaussian function in Eq. (3). Therefore, this work will focus on the use of a Gaussian function as an example of a distribution function in DAEM.

Numerical Approach Strategy

Solving DAEM can be done by multiple approaches. The first approach is by using a model-free methodology. This approach was further developed some years ago under the name of Miura-Maki approximation [26-28]. The latter is carried out by direct numerical calculation. Solving the DAEM with numerical calculation needs a certain kind of strategy to tackle the double integration with respect to temperature and activation energy. In this work, to familiarize and simplify our methodology, we implemented a trapezoidal rule in Eq. (4) to solve the integration.

$$\int_{x_0}^{x_n} f(x)dx = \frac{x_n - x_0}{n - 1} \cdot [f(x_0) + 2 \cdot f(x_1) + \dots + 2 \cdot f(x_{n-1}) + f(x_n)] \tag{4}$$

In Eq. (4), the integral equation is solved by discretization, which requires the user to predetermine the number of increments. In terms of DAEM, the discretization should be done for the integration to temperature and activation energy. These integrations are conducted simultaneously and are a kind of strategy to solve it. Therefore, we developed an algorithm to address this challenge.

Figure 1 shows the overall algorithm to numerically solve DAEM. This algorithm is also supported by a subroutine algorithm for an integration to temperature, as shown in Figure 2. To begin with, the algorithm is started by setting the kinetics parameters that are needed to calculate the kinetic study. In this work, we used a pre-exponential factor with a value of $1.67 \times 10^{13} \, \text{s}^{-1}$, activation energy at 170 kJ mol⁻¹, and a standard deviation of the activation energy of 5 kJ mol⁻¹. Furthermore, for the heating rate we assumed the value to be 5 K min⁻¹.

The next step is to determine and discretize the activation energy integration range. For this, we introduce an adaptive lower and upper integration limit:

$$E_{span} = [\bar{E} - f \cdot \sigma \quad \bar{E} - f \cdot \sigma + \Delta E \quad \dots \quad \bar{E} + f \cdot \sigma - \Delta E \quad \bar{E} + f \cdot \sigma]$$
 (5)

As shown by Eq. (5), the lower limit is valued at mean activation energy subtracted by a certain factor multiplied by the standard deviation of the activation energy, while the upper limit is valued at mean activation energy plus a certain factor multiplied by the standard deviation of the activation energy.

In the third step, we need to determine which kind of DAEM equation we are going to use. In this stage, we use two kinds of conditions, i.e., a first-order DAEM as well as a nth order DAEM with 2 as the reaction order.

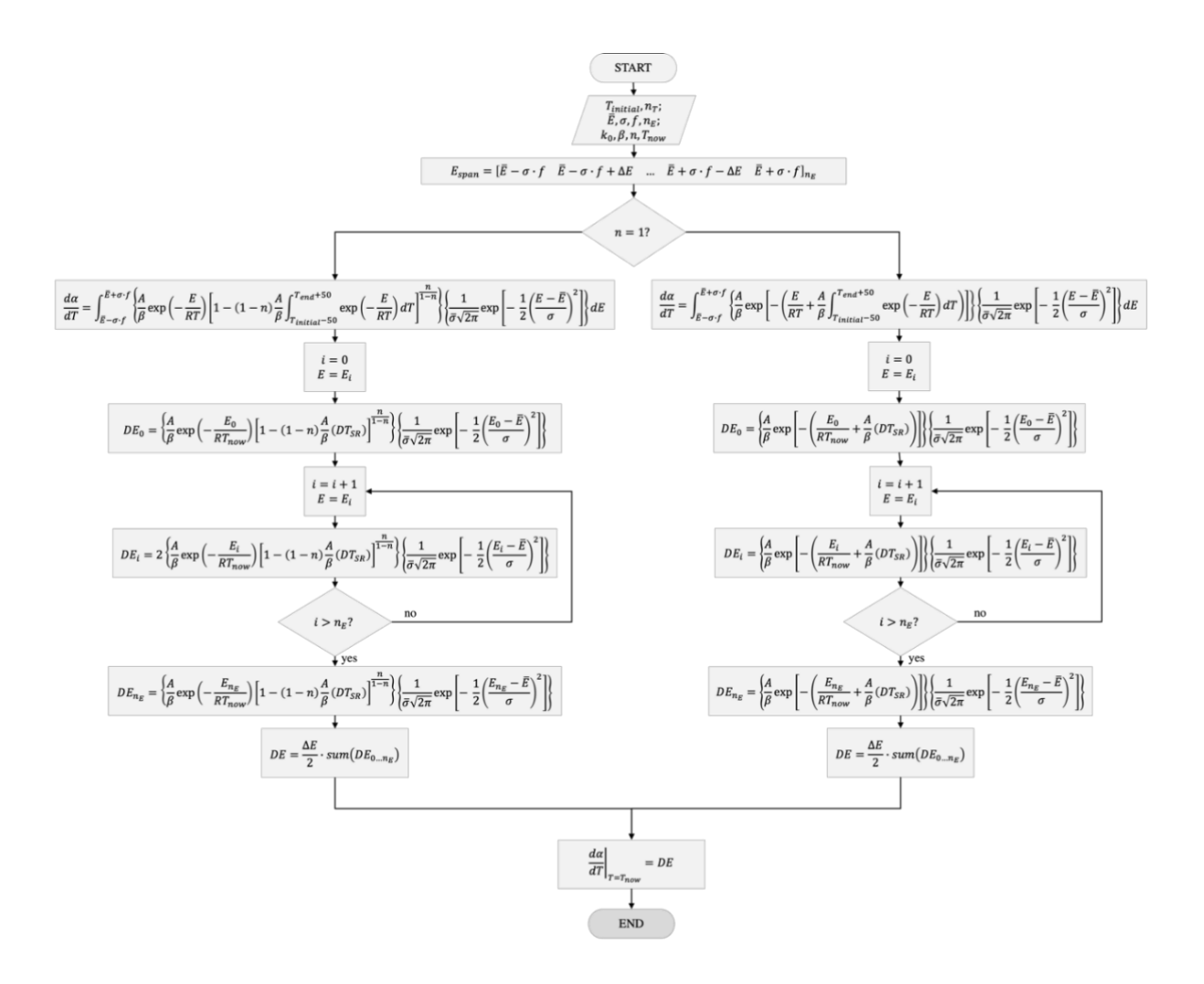


Figure 1 Overall algorithm of numerical method for solving 1st order and nth order DAEM.

The next stage is to calculate the DAEM with the trapezoidal integration methodology. In this stage, we need to set a certain activation energy value. The value will later be used to do a calculation in the DT subroutine to discretize the temperature integration range, as expressed in Eq. (6):

$$T_{span} = [473.15 \quad 473.15 + \Delta T \quad \dots \quad T_{now} - \Delta T \quad T_{now}]$$
 (6)

The lower limit of the temperature integration range was set at 200 $^{\circ}$ C (473.15 K). Meanwhile, the upper limit was capped at the temperature at which the rate of reaction is calculated. The results from this stage were summed up and multiplied by the delta value of the temperature integration point and divided by two; this calculation is called trapezoidal integration. The calculation was continued by at subsequent value of activation energies. The results were later calculated by the same trapezoidal integration to yield the intended value of the reaction rate.

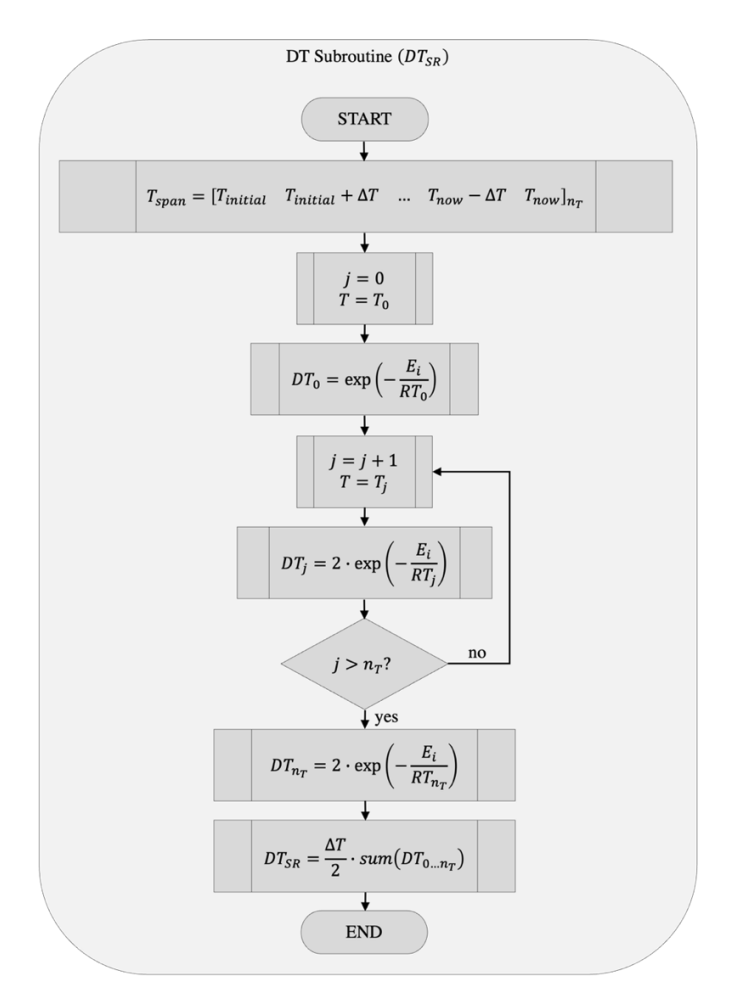


Figure 2 Sub-routine algorithm of numerical method for solving 1st order and nth order DAEM.

Statistical Comparison

The different configurations of the numerical methods presented in this work were compared to give an insight of their accuracy. The comparisons were conducted by using the sum squared of errors, a standardized and well-known statistical parameter in Eq. (7):

$$SSE = \sum \left[\left(\frac{d\alpha}{dT} \Big|_{base} - \frac{d\alpha}{dT} \Big|_{reviewed} \right)^2 \right]$$
 (7)

The calculation of SSE was conducted by subtracting the current reaction rate value that is being reviewed with a value that has been calculated by using a base configuration. The base configuration uses 251 temperature points, 251 temperature integration points, 251 activation energy integration points, and a value of 10 for the activation energy standard deviation factor for its integration limits.

Results and Discussion

Influence on the Number of Integration Points

Reviewing the number of integration points in DAEM can be divided into three parts. The first one is the number of observed temperature points where the reaction rate is measured, the second is the amount of discretization of the activation energy integration limit, and the last is the discretization of the temperature integration limit.

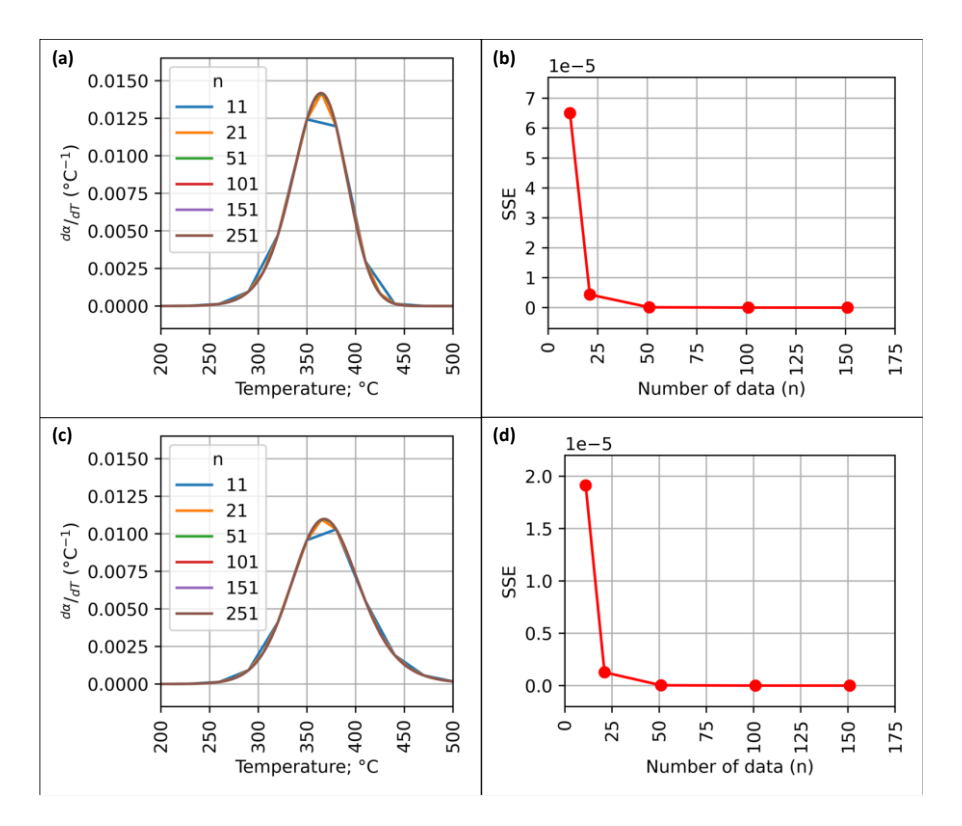


Figure 3 DTG and SSE curve of (a), (b) 1st order DAEM and (c), (d) 2nd order DAEM at various temperature data points.

In this first part, we varied the number of temperature data points to calculate the reaction rate with DAEM. Figure 3Error! Reference source not found.(a) and 3(c) show that using 11 and 21 data points resulted in a disproportionate graph. This result is also highlighted in Figure 3(b) and 3(d) where the SSE values are much higher relative to the other three alternatives. Hence, using 51 data points can be considered adequate to yield a proportional DTG curve. A higher number of data will increase the duration of the simulation as can be seen in Table 1. Nevertheless, an increase from 11 to 51 or even 101 data is considerably minimum. Therefore, using a higher number of temperature data points such as 51 and 101 is a good compromise between accuracy and simulation time.

Number of	First-order DAEM		n th -order DAEM		
Data; $oldsymbol{n}$	SSE	Simulation Time (s)	SSE	Simulation Time (s)	
11	6.50 x 10 ⁻⁵	1.06	1.91 x 10 ⁻⁵¹	1.06	
21	4.36 x 10 ⁻⁶	2.03	1.27 x 10 ⁻⁶¹	2.01	
51	1.15 x 10 ⁻⁷	4.87	3.31 x 10 ⁻⁸¹	4.86	
101	7.19 x 10 ⁻⁹	9.69	2.07 x 10 ⁻⁹¹	9.66	
151	1.42 x 10 ⁻⁹	14.38	4.09 x 10 ⁻¹⁰	14.38	
251	_	23 04	_	24.00	

Table 1 SSE and simulation time at various temperature data points.

In the second part, the number of activation energy integration points was varied. Figure 4(a) and (c) illustrate that the use of eleven points of integration generated an inordinate DTG curve. Comparably, the use of the same number of integration points also generated a much higher SSE than the other alternatives in Figure 4(b) and 4(d). Consequently, using 21 data points can be considered adequate to yield a satisfying DTG curve.

0.0150 0.00015 n_E 11 0.0125 21 0.0100 0.00010 51 101 0.0075 151 0.0050 0.00005 251 0.0025 0.0000 0.00000 500 50 100 Temperature; Number of data (n_E) (c) (d) 1e-5 0.0150 1.2 11 0.0125 21 1.0 0.0100 51 0.8 101 0.0075 9.0 151 0.0050 251 0.4 0.0025 0.2

0.0000 0.0 25 250 300 400 50 100 Temperature; °C Number of data (n_E)

Figure 4 DTG and SSE curve of (a), (b) 1st order DAEM and (c), (d) 2nd order DAEM at various activation energy integration points.

Using a higher number of data will increase the duration of the simulation, as can be seen in Table 2. The same as found in the first part of this section, the increase of the simulation time from 11 to 101 data is considerably minimum. Hence, to achieve a good compromise between the value of SSE and the duration of the simulation, the use of 21 or 51 integration points for the activation energy is sufficient.

Number of Integration Daint, a	First-order DAEM		n th -order DAEM	
Number of Integration Point; n	SSE	Simulation Time (s)	SSE	Simulation Time (s)
11	1.18 x 10 ⁻⁴¹	1.18	1.22 x 10 ⁻⁵¹	1.11
21	7.01 x 10 ⁻⁹¹	2.23	7.53 x 10 ⁻¹³	2.06
51	6.07 x 10 ⁻²³	4.84	1.29 x 10 ⁻³⁰	4.85
101	1.71 x 10 ⁻³⁰	9.65	1.28 x 10 ⁻³⁰	9.55
151	4.38 x 10 ⁻³¹	14.24	3.28 x 10 ⁻³¹	14.50
251	-	23.94	-	24.00

Table 2 SSE and simulation time at various activation energy integration points.

The last part of this subsection discusses the selection of temperature integration points. Figure 5(a) and 5(c) show that the use 11 and 21 integration points resulted in a DTG curve that slightly deviates from the correct value. This also resulted in a much higher SSE than the other alternatives as can be seen in Figure 5(b) and 5(d). Thus, using 51 points of data can be considered adequate to yield a satisfying DTG curve.

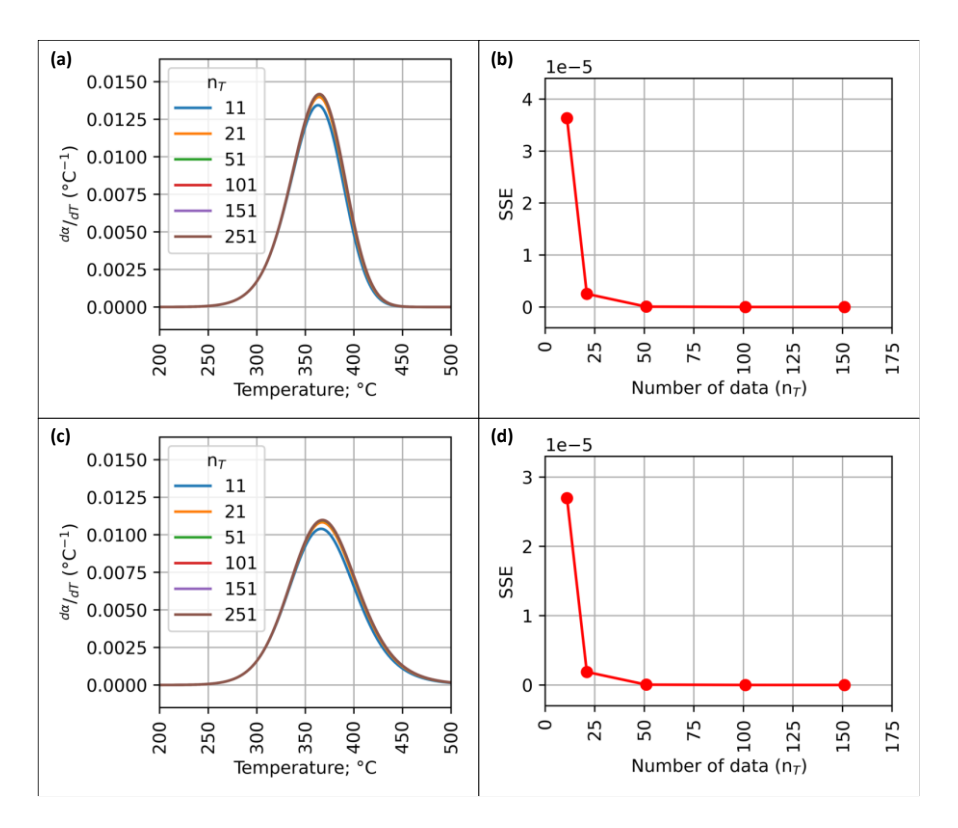


Figure 5 DTG and SSE curve of (a), (b) 1st order DAEM and (c), (d) 2nd order DAEM at various activation temperature integration points.

In Table 3, the increase of the simulation time from 11 to 101 once again can be considered as minimum. By weighing two factors, i.e., the value of SSE and the duration of the simulation, the use of 51 or 101 temperature points of integration are sufficient.

From the exploration of the temperature data points and the number of integration points for activation energy and temperature, it can be concluded that the minimum requirement to generate a satisfying DTG curve from first-order and nth-order DAEMs is:

- 1. the number of temperature data points must be above 51,
- 2. the number of activation energy integration points must be above 21,
- 3. the number of temperature integration points must be above 51.

Number of Internation Daint.	First-order DAEM		n th -order DAEM	
Number of Integration Point; n	SSE	Simulation Time (s)	SSE	Simulation Time (s)
11	3.63 x 10 ⁻⁵¹	1.10	2.70 x 10 ⁻⁵¹	1.05
21	2.52 x 10 ⁻⁶¹	1.99	1.88 x 10 ⁻⁶¹	1.98
51	6.24 x 10 ⁻⁸¹	4.79	4.66 x 10 ⁻⁸¹	4.85
101	3.00 x 10 ⁻⁹¹	9.70	2.24 x 10 ⁻⁹¹	9.48
151	3.44 x 10 ⁻¹⁰	14.13	2.57 x 10 ⁻¹⁰	14.33

 Table 3
 SSE and simulation time at various temperature integration points.

However, to increase the accuracy of the rest of the subsections, we increase the value of these three parameters by one degree, as follows:

23.94

24.00

1. the number of temperature data points = 101,

251

- 2. the number of activation energy integration points = 51,
- 3. the number of temperature integration point s = 101.

Influence of Adaptive Integration Limits

The integration limit of the activation energy is crucial to generate a suitable DTG curve from a DAEM. In the original form of the DAEM, the integration limit of activation energy starts from 0 and ends at a value of ∞ . This integration limit is unpractical and requires a lot of computational power. Therefore, to simplify the integration of DAEM, we tried to implement an adaptive limit for activation energy integration.

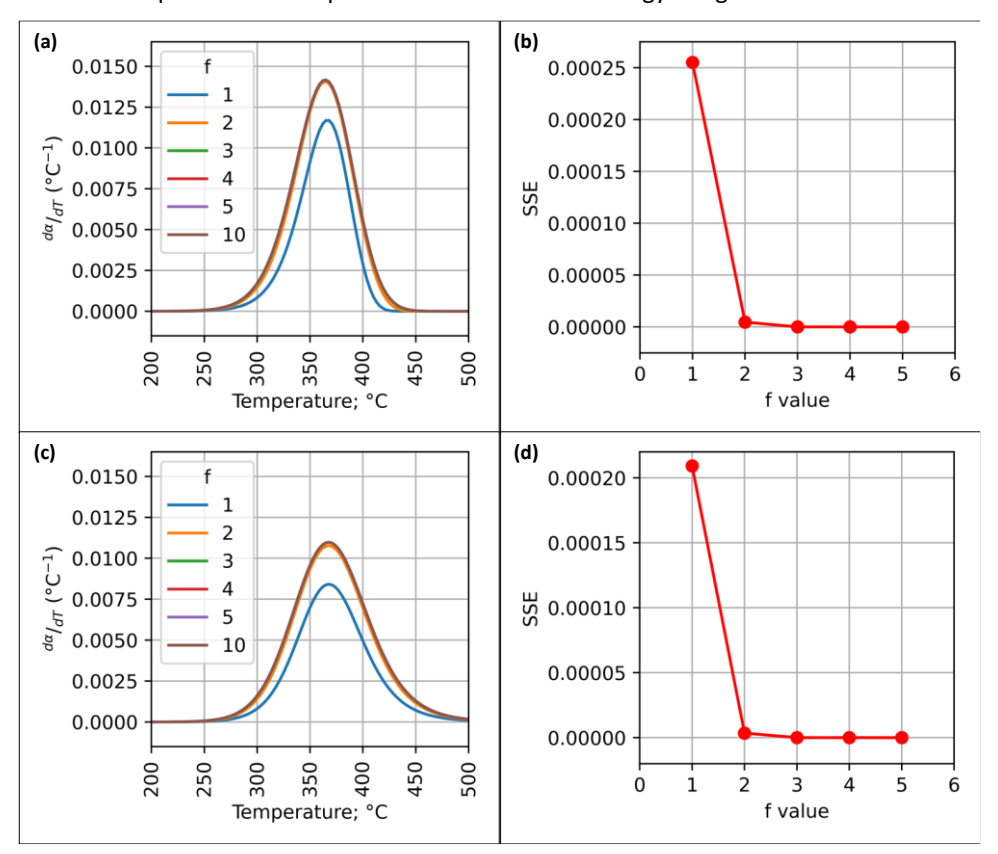


Figure 6 DTG and SSE curve of (a), (b) 1^{st} order DAEM and (c), (d) 2^{nd} order DAEM at various activation energy integration limits.

The adaptive integration limit for activation energy was based on the value of its mean activation energy and its standard deviation value. Here, we varied it between the value of mean activation energy subtracted by the standard deviation and five times its standard deviation. To compare between the alternatives, we still used the value of ten times the standard deviation as the base calculation.

Figure 6(a) and 6(c) show the different shapes of the DTG curve at different integration limits. The value of one and two times the standard deviation resulted in an off-shape DTG curve. As presented in Figure 6(b) and 6(d), the SSE value of these two configurations was also much higher than that of the other integration setups. Subsequently, the use of an integration limit for the activation energy minus three times the standard deviation of the activation energy plus three times the standard deviation gave a satisfying result.

Influence of Heating Rates

After setting the optimal configuration to calculate the DAEM, we tried to explore the application of a DAEM in thermogravimetric pyrolysis experiments. In a kinetic study of thermogravimetric pyrolysis, it is common to vary the heating rate to obtain the kinetic parameters. This approach is usually found in model-free kinetic studies [27,29,30]. However, in model-fitting kinetic studies, the search for the kinetic parameters often only involves one heating rate [20,23,25]. Therefore, in this work, we investigated the effect of the heating rate on the shape of the DAEM curve.

In thermogravimetric pyrolysis, the heating rate has been proven to affect the shape of the reaction, where thermogravimetric pyrolysis with a higher heating rate usually pushes the reaction peak to a higher temperature [18,31]. The delayed reaction peak is commonly subjected to thermal lag or thermal hysteresis, where the temperature of the sample is lower than the temperature measured by the instrument. This often found in low thermal conductivity samples such as solid biomass [32,33].

The shift of the reaction peak in thermogravimetric pyrolysis under various heating rates can be modeled with DAEM. In DAEM, the heating rate is found as the denominator of the preexponential factor as presented in Eqs. (1) and (2) Thus, higher heating rates must have reduced the value of the reaction rate. In Figure 7(a) and 7(b), a DAEM with higher heating rates at the same kinetic parameters resulted in a shift of the reaction peaks towards a higher temperature. At the same time, the peak of the reaction was also reduced by a certain magnitude.

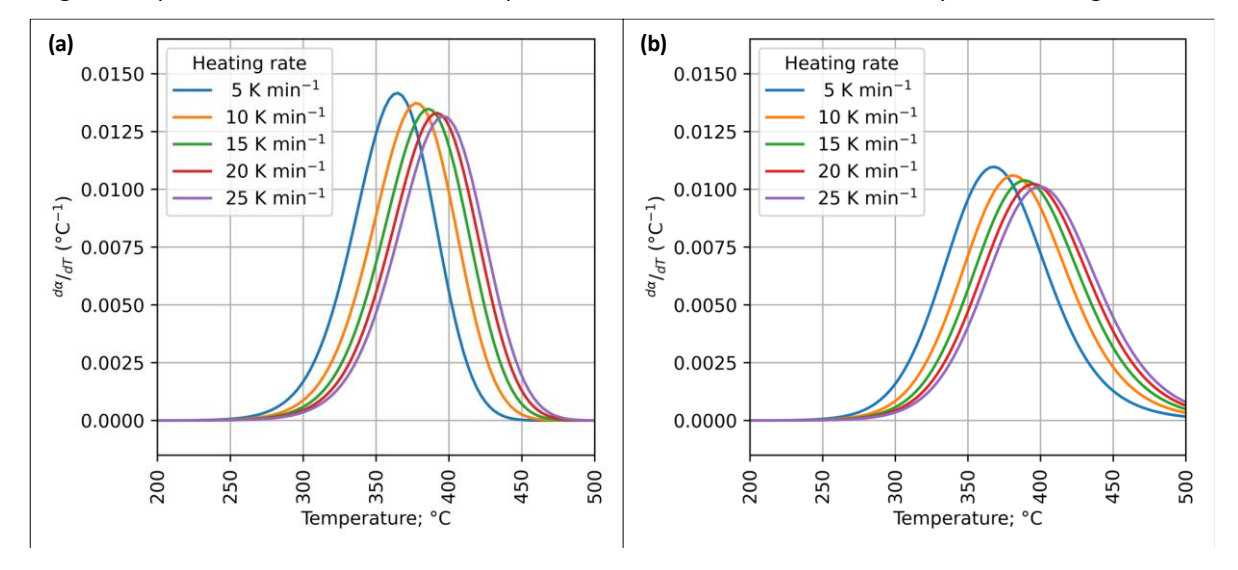


Figure 7 DTG curve of (a) 1st order DAEM and (c) 2nd order DAEM at various heating rates.

A decline in the reaction rate peak has been found in several previous studies, for instance, for the pyrolysis of teak sawdust [18], cellulose [34, 35], poplar wood sawdust [36], and Chinese herb residues [30]. By comparing the nature of DAEM and these findings in previous research, it can be expected that that the DAEM has the ability to model the reaction curve of biomass thermogravimetric pyrolysis.

General Strategy to Obtain Reliable Kinetic Parameters

We have investigated and explored the use of DAEM in our previous modeling of thermogravimetric pyrolysis experiment [18,20]. From the findings and this work, it can be concluded that the number of data points and integration points, and the integration range are important to generate a proportional DAEM curve. In Figure 8(a) and 8(b), we can see that the use of an optimal configuration was able to produce a proportional DTG curve compared to the base calculation configuration. From our measurement, the optimal calculation configuration only needs 0.9 seconds to complete. This value is much lower than the base calculation configuration, which needs about 24 seconds to complete. In a nutshell, using the optimal configuration for the numerical calculation increases our calculation efficiency about 25-fold compared to using the base configuration with the same accuracy.

In more detail, Figure 8(c) and 8(d) show the peak area of both calculation configurations. As presented in that figure, there are slight differences in the reaction rate value between the base calculation and the optimal calculation configuration. However, the differences can be considered miniscule and negligible. Therefore, the optimal configuration that we found can be considered as a good way to directly compute DAEM with numerical methods.

DOI: 10.5614/j.eng.technol.sci.2023.55.3.4

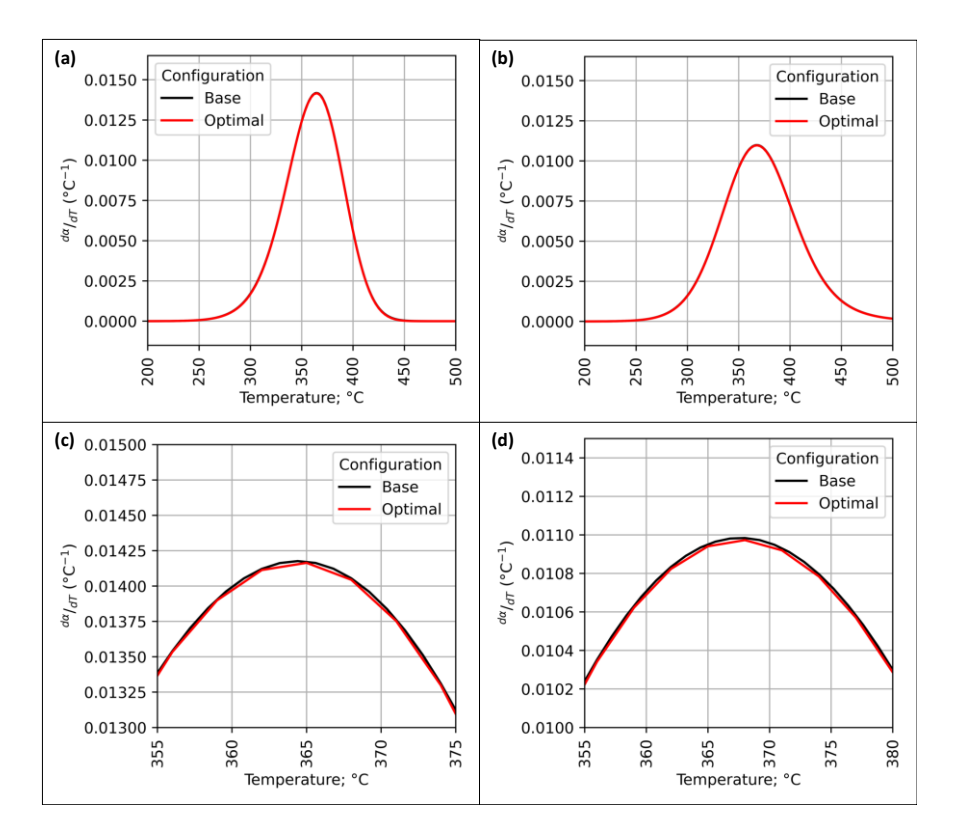


Figure 8 DTG and DTG peak curve comparison of (a), (b) 1^{st} order DAEM and (c), (d) 2^{nd} order DAEM at base and optimal numerical calculation configuration.

This direct numerical calculation of DAEM with an optimal configuration can be directly implemented in a kinetic study of thermogravimetric pyrolysis at various heating rates. As previously highlighted in Section 3.3 and Figure 7, it is possible to model thermogravimetric pyrolysis with DAEM under many different heating rates. This approach is still limited since most model-fitting kinetic studies of biomass pyrolysis using DAEM were only conducted by involving a single heating rate experiment [20,23,25]. In our previous study, we explored the possibility of using multi-distribution DAEM on a kinetics study of teak sawdust, lignin, and cellulose at three different heating rates [18]. From that work, we consider that multiple heating rates can provide more consistent kinetic parameters. This simultaneously proves that small changes of the heating rate have minimal or no impact on the type of reaction in thermogravimetric pyrolysis. Additionally, the addition of an extra parameter of extent of reaction in DAEM has the potential to elucidate the role of metal [1] or non-metallic [2] catalysts in pyrolysis to produce a more favorable product.

Conclusions

DAEM is one of many forms of model-fitting kinetic analysis of thermogravimetric pyrolysis of biomass. To model the reaction rate or DTG curve for thermogravimetric pyrolysis, DAEM should be calculated in such a way that it can produce an accurate and proportional result. In this paper, the optimal configuration to calculate DAEM is given. It turned out that the optimal number of temperature data points should be at least 51 points, while the number of activation energy and temperature integration points must be above 21 and 51 points, respectively. Meanwhile, in terms of the activation energy integration limit, an adaptive integration limit should be applied. The range is recommended to span from mean activation energy minus three times its standard deviation to mean activation energy plus three times its standard deviation. By using this configuration, one can achieve a proportional and suitable DAEM curve to fit experimental DTG curves.

The use of DAEM in multi-heating rate thermogravimetric pyrolysis was also highlighted in this work. A higher heating rate will generate a proportional shift of the reaction peak towards a higher temperature, which has been found in several other studies. Therefore, it is possible to implement DAEM in kinetic studies by using multiple heating rates of thermogravimetric pyrolysis.

Acknowledgement

We thank the Directorate General of Higher Education, Research and Technology, Ministry Education, Culture, Research & Technology of the Republic of Indonesia (*Kementerian Pendidikan, Kebudayaan, Riset, dan Teknologi, Republik Indonesia*) for their support through funding number 018/E5/PG.02.00.PT/2022.

References

- [1] Puspawiningtiyas, E., Prakoso, T., Pratiwi, M., Subagjo, S. & Soerawidjaja, T.H., *Production of Biogasoline via Pyrolysis of Oleic Acid Basic Soaps,* Journal of Engineering and Technological Sciences, **54**, 220311, 2022. doi: 10.5614/j.eng.technol.sci.2022.54.3.11.
- [2] Irawan, A., Bindar, Y., Kurniawan, T., Alwan, H., Rosid, R. & Fauziah, N.A., *Bayah Natural Zeolites to Upgrade the Quality of Bio Crude Oil from Empty Fruit Bunch Pyrolysis*, Journal of Engineering and Technological Sciences, **53**, 210308, 2021. doi: 10.5614/j.eng.technol.sci.2021.53.3.8.
- [3] Ro, D., Kim, Y.-M., Lee, I.-G., Jae, J., Jung, S.-C., Kim, S. C. & Park, Y.-K., Bench Scale Catalytic Fast Pyrolysis of empty Fruit Bunches over Low Cost Catalysts And HZSM-5 Using a Fixed Bed Reactor, Journal of Cleaner Production, **176**, pp. 298-303, 2018. doi: 10.1016/j.jclepro.2017.12.075.
- [4] Zhang, H., Xiao, R., Wang, D., He, G., Shao, S., Zhang, J. & Zhong, Z., *Biomass Fast Pyrolysis in a Fluidized Bed Reactor Under N2, CO2, CO, CH4 And H2 Atmospheres, Bioresour Technol,* **102**, pp. 4258-4264, 2011. doi: 10.1016/j.biortech.2010.12.075.
- [5] Wintoko, J., Purwono, S., Fahrurrozi, M. & Soehendro, B., *Analysis Method of Black Liquor Pyrolysis and Gasification Using Deconvolution Technique to Obtain the Real Time Gas Production Profile*, Jurnal Rekayasa Proses, **14**, pp.19-29, 2020. doi: 10.22146/jrekpros.56152.
- [6] Jamilatun, S., Budiman, A., Mufandi, I., Aktawan, A., Fauzi, N. & Denanti, D.P., *The Effects of Particle Mesh and Temperature on Pyrolysis Spirulina platensis Residue (SPR): Pyrolysis Yield and Bio-Oil Properties*, ASEAN Journal of Chemical Engineering, **22**, pp.141-155, 2022. doi: 10.22146/ajche.69439
- [7] Vyazovkin, S., Burnham, A.K., Favergeon, L., Koga, N., Moukhina, E., Pérez-Maqueda, L. A. & Sbirrazzuoli, N., ICTAC Kinetics Committee Recommendations for Analysis of Multi-step Kinetics, Thermochimica Acta, 689, 178597, 2020. doi: 10.1016/j.tca.2020.178597.
- [8] Jain, A.A., Mehra, A. & Ranade, V.V., *Processing of TGA data: Analysis of Isoconversional and Model Fitting Methods*, Fuel, **165**, pp. 490-498, 2016. doi: 10.1016/j.fuel.2015.10.042.
- [9] Loy, A.C.M., Gan, D.K.W., Yusup, S., Chin, B.L.F., Lam, M.K., Shahbaz, M., Unrean, P., Acda, M.N. & Rianawati, E., *Thermogravimetric Kinetic Modelling of In-Situ Catalytic Pyrolytic Conversion of Rice Husk To Bioenergy Using Rice Hull Ash Catalyst*, Bioresour Technol, **261**, pp. 213-222, 2018. doi: 10.1016/j.biortech.2018.04.020.
- [10] Jia, C., Chen, J., Bai, J., Yang, X., Song, S. & Wang, Q., Kinetics of the Pyrolysis of Oil Sands Based Upon Thermogravimetric Analysis, Thermochimica Acta, 666, pp. 66-74, 2018. doi: 10.1016/j.tca.2018.06.002
- [11] Nawaz, A., Mishra, R. K., Sabbarwal, S. & Kumar, P., Studies of Physicochemical Characterization and Pyrolysis Behavior of Low-Value Waste Biomass Using Thermogravimetric Analyzer: Evaluation of Kinetic and Thermodynamic Parameters, Bioresource Technology Reports, 16, 100858, 2021. doi: 10.1016/j.biteb.2021.100858.
- [12] Nawaz, A. & Kumar, P., Impact of Temperature Severity on Hydrothermal Carbonization: Fuel Properties, Kinetic and Thermodynamic Parameters, Fuel, **336**, 127166, 2023. doi: 10.1016/j.fuel.2022.127166
- [13] Nawaz, A. & Kumar, P., Elucidating the Bioenergy Potential of Raw, Hydrothermally Carbonized and Torrefied Waste Arundo Donax Biomass in Terms of Physicochemical Characterization, Kinetic and Thermodynamic Parameters, Renewable Energy, 187, pp. 844-856, 2022. doi: 10.1016/j.renene.2022.01.102.
- [14] Nawaz, A. & Kumar, P., *Pyrolysis of Mustard Straw: Evaluation of Optimum Process Parameters, Kinetic and Thermodynamic Study*, Bioresour Technol, **340**, 125722, 2021. doi: 10.1016/j.biortech.2021.125722
- [15] Vyazovkin, S., Burnham, A.K., Criado, J.M., Pérez-Maqueda, L.A., Popescu, C. & Sbirrazzuoli, N., ICTAC Kinetics Committee Recommendations for Performing Kinetic Computations on Thermal Analysis Data, Thermochimica Acta, **520**, pp. 1-19, 2011. doi: 10.1016/j.tca.2011.03.034.
- [16] Hernowo, P., Rasrendra, C.B., Budhi, Y.W., Rizkiana, J., Irawan, A., Marno, S., Meliana, Y., Muraza, O. & Bindar, Y., Volatile State Mathematical Models for Predicting Components in Biomass Pyrolysis Products,

DOI: 10.5614/j.eng.technol.sci.2023.55.3.4

- Journal of Engineering and Technological Sciences, **54**, 220108, 2022. doi: 10.5614/j.eng.technol.sci.2022.54.1.8.
- [17] Aswie, V., Qadariyah, L. & Mahfud, M., *Kinetics and Characterization of Microalgae Biofuel by Microwave-assisted Pyrolysis Using Activated Carbon,* Journal of Engineering and Technological Sciences, **54**, 220207 2022. doi: 10.5614/j.eng.technol.sci.2022.54.2.7.
- [18] Kristanto, J., Daniyal, A.F., Pratama, D.Y., Bening, I.N.M., Setiawan, L., Azis, M.M. & Purwono, S., *Kinetic Study on the Slow Pyrolysis of Isolated Cellulose and Lignin from Teak Sawdust*, Thermochimica Acta, **711**, pp., 2022. doi: 10.1016/j.tca.2022.179202.
- [19] Cai, J., Wu, W. & Liu, R., An Overview of Distributed Activation Energy Model and Its Application in the Pyrolysis of Lignocellulosic Biomass, Renewable and Sustainable Energy Reviews, **36**, pp. 236-246, 2014. doi: 10.1016/j.rser.2014.04.052.
- [20] Kristanto, J., Azis, M.M. & Purwono, S., *Multi-distribution Activation Energy Model on Slow Pyrolysis of Cellulose and Lignin In TGA/DSC*, Heliyon, **7**, e07669, 2021. doi: 10.1016/j.heliyon.2021.e07669.
- [21] Liu, H., Ahmad, M.S., Alhumade, H., Elkamel, A. & Cattolica, R.J., *Three Pseudo-Components Kinetic Modeling and Nonlinear Dynamic Optimization of Rhus Typhina Pyrolysis with the Distributed Activation Energy Model*, Applied Thermal Engineering, **157**, 113633, 2019. doi: 10.1016/j.applthermaleng.2019.04.043.
- [22] Wu, W., Mei, Y., Zhang, L., Liu, R. & Cai, J., *Kinetics and Reaction Chemistry of Pyrolysis and Combustion of Tobacco Waste*, Fuel, **156**, pp. 71-80, 2015. doi: 10.1016/j.fuel.2015.04.016.
- [23] Zhang, J., Chen, T., Wu, J. & Wu, J., *Multi-Gaussian-DAEM-Reaction Model for Thermal Decompositions of Cellulose, Hemicellulose and Lignin: Comparison of N(2) and CO(2) Atmosphere*, Bioresour Technol, **166**, pp. 87-95, 2014. doi: 10.1016/j.biortech.2014.05.030.
- [24] Gunes, M. & Gunes, S., A Direct Search Method for Determination of DAEM Kinetic Parameters from Nonisothermal TGA Data (Note), Applied Mathematics and Computation 130, pp. 619-628, 2002. doi: 10.1021/ie980601n.
- [25] Cai, J., Wu, W., Liu, R. & Huber, G.W., A Distributed Activation Energy Model for the Pyrolysis of Lignocellulosic Biomass, Green Chemistry, 15, pp.1331-1340, 2013. doi: 10.1039/c3gc36958g.
- [26] Wintoko, J., Purwono, S., Fahrurrozi, M. & Soehendro, B., *Black Liquor Droplet Swelling Model during Pyrolysis*, IOP Conference Series: Materials Science and Engineering, 26th Regional Symposium on Chemical Engineering (RSCE 2019) 30-31 October 2019, Kuala Lumpur, Malaysia, **778**, 012109, 2019.
- [27] Yang, H., Ji, G., Clough, P.T., Xu, X. & Zhao, M., *Kinetics of Catalytic Biomass Pyrolysis Using Ni-Based Functional Materials,* Fuel Processing Technology, **195**, 106145, 2019. doi: 10.1016/j.fuproc.2019.106145
- [28] Fiori, L., Valbusa, M., Lorenzi, D. & Fambri, L., *Modeling of the Devolatilization Kinetics during Pyrolysis of Grape Residues*, Bioresour Technol, **103**, pp. 389-397, 2012. doi: 10.1016/j.biortech.2011.09.113.
- [29] Altarawneh, S., Al-Harahsheh, M., Dodds, C., Buttress, A. & Kingman, S., *Thermal Degradation Kinetics of Polyvinyl Chloride in Presence of Zinc Oxide*. Thermochimica Acta, **707**, 179105., 2022. doi: 10.1016/j.tca.2021.179105.
- [30] Huang, S., Su, Y., Luo, W., He, Q., Huang, S., Zhou, N. & Zhou, Z., *Kinetic Analysis and In-Situ No Support Catalytic Pyrolysis Product Distribution of Chinese Herb Residue*, Journal of Analytical and Applied Pyrolysis, **156**(12), 105114, 2021. doi: 10.1016/j.jaap.2021.105114.
- [31] Su, D., Chen, X., Wei, X., Liang, J., Tang, L. & Wang, L., Comparison of Thermal Stability Between Dicyclopentadiene/Hydrogenated Dicyclopentadiene Petroleum Resin: Thermal Decomposition Characteristics, Kinetics and Evolved Gas Analysis By TGA/TG-MS, Thermochimica Acta, 699, 178853, 2021. doi: 10.1016/j.tca.2020.178853.
- [32] Chen, X., Li, S., Liu, Z., Chen, Y., Yang, H., Wang, X., Che, Q., Chen, W. & Chen, H., *Pyrolysis Characteristics of Lignocellulosic Biomass Components in the Presence of Cao*, Bioresour Technol, **287**, 121493, 2019. doi: 10.1016/j.biortech.2019.121493.
- [33] Sharma, P., Pandey, O.P. & Diwan, P.K., *Non-Isothermal Kinetics of Pseudo-Components of Waste Biomass*, Fuel, **253**, pp. 1149-1161, 2019. doi: 10.1016/j.fuel.2019.05.093.
- [34] Jiang, L. Q., Lin, Q., Lin, Y., Xu, F.X., Zhang, X., Zhao, Z.L. & Li, H.B., Impact of Ball-Milling and Ionic Liquid Pretreatments on Pyrolysis Kinetics and Behaviors of Crystalline Cellulose, Bioresour Technol, **305**, 123044, 2020. doi: 10.1016/j.biortech.2020.123044.
- [35] Chen, W.-H., Eng, C.F., Lin, Y.-Y. & Bach, Q.-V., *Independent Parallel Pyrolysis Kinetics of Cellulose, Hemicelluloses and Lignin at Various Heating Rates Analyzed by Evolutionary Computation,* Energy Conversion and Management, **221**, 113165, 2020. doi: 10.1016/j.enconman.2020.113165.

[36] Hu, M., Chen, Z., Wang, S., Guo, D., Ma, C., Zhou, Y., Chen, J., Laghari, M., Fazal, S., Xiao, B., Zhang, B. & Ma, S., *Thermogravimetric Kinetics of Lignocellulosic Biomass Slow Pyrolysis Using Distributed Activation Energy Model, Fraser–Suzuki Deconvolution, and Iso-Conversional Method,* Energy Conversion and Management, **118**, pp. 1-11, 2016. doi: 10.1016/j.enconman.2016.03.058.